BIOLOGY OF REPRODUCTION (2015) **92**(6):146, 1–14
Published online before print 22 April 2015.
DOI 10.1095/biolreprod.114.127027

MAPK3/1 (ERK1/2) and Myosin Light Chain Kinase in Mammalian Eggs Affect Myosin-II Function and Regulate the Metaphase II State in a Calcium- and Zinc-Dependent Manner[1]

Lauren A. McGinnis,[3] Hyo J. Lee,[3] Douglas N. Robinson,[4] and Janice P. Evans[2,3]

[3]*Department of Biochemistry and Molecular Biology, Bloomberg School of Public Health, Johns Hopkins University, Baltimore, Maryland*
[4]*Department of Cell Biology, School of Medicine, Johns Hopkins University, Baltimore, Maryland*

ABSTRACT

Vertebrate eggs are arrested at metaphase of meiosis II, a state classically known as cytostatic factor arrest. Maintenance of this arrest until the time of fertilization and then fertilization-induced exit from metaphase II are crucial for reproductive success. Another key aspect of this meiotic arrest and exit is regulation of the metaphase II spindle, which must be appropriately localized adjacent to the egg cortex during metaphase II and then progress into successful asymmetric cytokinesis to produce the second polar body. This study examined the mitogen-activated protein kinases MAPK3 and MAPK1 (also known as ERK1/2) as regulators of these two related aspects of mammalian egg biology, specifically testing whether this MAPK pathway affected myosin-II function and whether myosin-II perturbation would produce some of the same effects as MAPK pathway perturbation. Inhibition of the MEK1/2-MAPK pathway with U0126 leads to reduced levels of phosphorylated myosin-regulatory light chain (pMRLC) and causes a reduction in cortical tension, effects that are mimicked by treatment with the myosin light chain kinase (MLCK) inhibitor ML-7. These data indicate that one mechanism by which the MAPK pathway acts in eggs is by affecting myosin-II function. We further show that MAPK or MLCK inhibition induces loss of normal cortical spindle localization or parthenogenetic egg activation. This parthenogenesis is dependent on cytosolic and extracellular calcium and can be rescued by hyperloading eggs with zinc, suggesting that these effects of inhibition of MLCK or the MAPK pathway are linked with dysregulation of ion homeostasis.

calcium, cytoskeleton, egg activation, MAPK, myosin-II, parthenogenesis, spindle, zinc

INTRODUCTION

Vertebrate eggs are arrested at metaphase of meiosis II, a state classically known as cytostatic factor arrest [1]. Completion of meiosis is normally triggered by the fertilizing sperm; this exit from metaphase II arrest is known as egg activation. Inability to exit from metaphase II arrest upon fertilization is associated with female infertility [2, 3]. Proper maintenance of metaphase II arrest in unfertilized eggs is also crucial for reproductive success, with failure of eggs to maintain metaphase II arrest being associated with reduced female fertility [4–7]. Reduced ability to maintain metaphase II arrest is also observed in eggs with down-regulated activity of endogenous meiotic inhibitor 2 (EMI2), CDC25A, or PP2A, with reduced levels of cytosolic zinc, or undergoing postovulatory aging [8–15]. A related crucial component of the metaphase II state is spatial control of the meiotic spindle to maintain spindle integrity and set up the asymmetric cytokinesis of second polar body emission. Defects in cytokinesis and the segregation of oocyte cytoplasmic components are associated with reduced female fertility (e.g., [16–20]). These temporal and spatial aspects of the metaphase II egg are controlled by interconnected machinery, and our work here has focused on the MAPK pathway, specifically MAPK1 (mitogen-activated protein kinase 1, also known as p42mapk or ERK2) and MAPK3 (mitogen-activated kinase 3, also known as ERK1 or p44erk1).

Control of the metaphase II state in vertebrate eggs is achieved on multiple levels. Sustained cyclin-dependent kinase 1 (CDK1) activity in the metaphase II egg maintains M-phase, and decreased CDK1 activity helps mediate exit from metaphase II. A complementary level of control is mediated by the anaphase-promoting complex (APC) [21, 22]. The APC is a multimeric E3 ubiquitin ligase; its substrates include cyclin B1 and securin, which are targeted for 26S proteasomal degradation upon ubiquitylation [21, 23]. APC activity is suppressed in the metaphase II egg, then the APC becomes active upon metaphase II exit. The protein EMI2 (endogenous meiotic inhibitor 2, also known as FBXO43) controls the inactive state of the APC in metaphase II [8, 24]. EMI2 is regulated by zinc and by the Mos-MEK-MAPK pathway. The Mos-MEK-MAPK pathway is essential for metaphase II arrest; oocytes from *mos*$^{-/-}$ mice and eggs treated with the MEK1/2 inhibitor U0126 undergo parthenogenetic activation [4–6, 25–27]. U0126-induced parthenogenesis is characterized by CDK1 inactivation and reduced phosphorylation of EMI2 [26, 28]. Parthenogenetic exit from metaphase II is also induced in eggs treated with the zinc chelator TPEN [11–13]. TPEN-induced parthenogenetic activation is prevented by overexpressing EMI2; this rescue appears to be dependent on zinc binding to EMI2 because overexpression of EMI2 with a mutation of a residue in the zinc-binding domain has significantly less of this preventative effect [29].

Calcium is another major factor controlling exit from metaphase II (reviewed in [30, 31]). In mouse eggs, calcium works through calcium/calmodulin-dependent kinase IIγ (CaMKIIγ, also known as CAMK2G) [2, 32]. EMI2 appears

[1]This work was supported by R03 HD074773 from the NIH to J.P.E. and D.N.R. H.J.L. was partially supported by the Sommer Scholarship from the Johns Hopkins Bloomberg School of Public Health.
[2]Correspondence: Janice P. Evans, Department of Biochemistry and Molecular Biology, Bloomberg School of Public Health, 615 N. Wolfe St., Johns Hopkins University, Baltimore, MD 21205.
E-mail: jevans6@jhu.edu

Received: 26 November 2014.
First decision: 30 December 2014.
Accepted: 16 April 2015.

eISSN: 1529-7268 http://www.biolreprod.org
ISSN: 0006-3363

to be a substrate for CaMKIIγ in mouse eggs [33], and based on what is known from *Xenopus,* this phosphorylation of EMI2 primes EMI2 for degradation [24, 34]. Interestingly, zinc loss from the egg is associated with increased cytosolic calcium. Fertilization and parthenogenesis induced by reagents that increase cytosolic calcium (e.g., $SrCl_2$, calcium ionophore) are accompanied by bursts of efflux of zinc, called zinc sparks, and this zinc efflux seems to be required for inactivation of EMI2 and subsequent activation of the APC [12, 13].

Transitions in the meiotic cell cycle must be coordinated with the function of the metaphase II spindle and cortical cytoskeleton, and the Mos-MEK-MAPK pathway also plays a role in this aspect of oocyte biology. MAPK is active through the two meiotic divisions in oocytes and remains high through egg activation after CDK1 activity has declined in fertilized eggs [35–38]. Mos-deficient oocytes and oocytes treated with U0126 during meiotic maturation have cortical cytoskeleton abnormalities and elongated metaphase I spindles that fail to migrate to the oocyte periphery, setting up aberrant cytokinesis in the first meiotic division [4–6, 25, 27, 39, 40]. Metaphase II eggs treated with U0126 develop abnormal spindles, including loss of normal localization adjacent to the egg cortex [37].

Our study here examines the connection between MAPK activity and cortical cytoskeleton function, testing the hypothesis that MAPK inhibition would result in abnormal function of nonmuscle myosin-II in metaphase II eggs. In other cell types, MAPK1/3 functions upstream of myosin light chain kinase (MLCK); MLCK phosphorylates myosin regulatory light chain (MRLC, also known as MYL9), which enables myosin-II organization into bipolar thick filaments [41–43]. Myosin-II functions in several events of the mammalian oocyte's meiotic transitions. The actomyosin cytoskeleton undergoes significant changes through meiosis I, with cortical tension and actin and myosin-II rearrangements mediating proper spindle positioning [40, 44, 45]. In meiosis I, MLCK inhibition and other myosin perturbations impair spindle migration and first polar body emission [40, 46, 47]. In metaphase II eggs, suppression of MLCK activity reduces cortical tension, inhibits DNA-induced remodeling of the cortical cytoskeleton, causes failure of postfertilization spindle rotation and second polar body emission, and impairs cortical granule exocytosis and sperm-triggered actomyosin cytoplasmic movements [44, 48–51]. The study here builds on our work showing that myosin-II-mediated cell mechanics in the egg cortex play a role in spindle function during exit from metaphase II [44] and tests the hypothesis that MEK-MAPK pathway perturbation affects myosin-II function in metaphase II eggs. These studies have uncovered new functions of the actomyosin cytoskeleton and the MEK-MAPK3/1-MLCK pathway in mammalian eggs.

MATERIALS AND METHODS

Collection and Manipulation of Ovulated Metaphase II Eggs

Animals were used in accordance with the guidelines of the Johns Hopkins University Animal Care and Use Committee. Ovulated metaphase II eggs were collected from 6- to 8-wk-old female CF-1 mice (Harlan) injected with 10 international units pregnant mare serum gonadotropin (Calbiochem/Millipore) 60 h prior to egg collection and then with 10 international units human chorionic gonadotropin (Sigma) 13–14 h prior to egg collection. Ovulated eggs were dissected from oviducts in Whitten's medium (109.5 mM NaCl, 4.7 mM KCl, 1.2 mM KH_2PO_4, 1.2 mM $MgSO_4$, 5.5 mM glucose, 0.23 mM pyruvic acid, 4.8 mM lactic acid hemicalcium salt [52]) supplemented with 7 mM $NaHCO_3$ and 15 mM HEPES (referred to hereafter as WH medium) and 0.025% Type IV-S hyaluronidase (Sigma) and 3 mg/ml bovine serum albumin (BSA) (Sigma). Cumulus-free eggs were washed through WH supplemented with 0.05% polyvinyl alcohol (referred to hereafter as WH/PVA) to remove residual hyaluronidase. The zonae pellucidae (ZP) were removed with a brief incubation (~10–15 sec) in acidic culture medium compatible buffer (116.4 mM NaCl, 5.4 mM KCl, 10 mM HEPES, 1 mM NaH_2PO_4, 0.8 mM $MgSO_4$, pH 1.5).

U0126 (Cell Signaling Technologies), which inhibits MEK1/2 (also known as mitogen-activated protein kinase kinase 1 and 2, or MAP2K1/2 [53]), was used to treat metaphase II eggs as previously described [26, 37, 54, 55]. U0126 was prepared as a 10 mM stock in dimethyl sulfoxide (DMSO) and used at a concentration 50 μM, which was based on previous work showing that parthenogenetic activation of eggs by U0126 was dose-dependent through 8 h of treatment, whereas 100 μM U0126 was cytotoxic to eggs [26]. The MLCK inhibitor ML-7 (Sigma; ML-7 also inhibits the skeletal muscle form, MYLK2) was used as previously described [44, 49]. ML-7 was prepared as a 10 mM stock in DMSO and used at a concentration 15 μM based on studies of the dose-dependence of ML-7 effects on metaphase II eggs [49]. DMSO at a concentration of 0.5% was used as a solvent control. DMSO, U0126, and ML-7 were diluted in WB/PVA for treatment of eggs; treatment times are specified in text and figure legends. ML-7 treatment was done in four-well Nunclon Δ-treated plates (Fisher Scientific) without mineral oil overlay as done previously [44, 49, 56]. Our attempts to disrupt myosin-II with blebbistatin have not been fruitful. For example, we observed that blebbistatin did not produce consistent effects on cortical tension in eggs, whereas ML-7 did [44]. This was consistent with reports that blebbistatin did not significantly inhibit polar body emission but ML-7 did [47], and is perhaps due to the propensity of blebbistatin to undergo photoinactivation [57].

For some experiments here, eggs were preloaded with the calcium chelator BAPTA-AM (Calbiochem) by culturing eggs in WB/PVA medium containing 5 μM BAPTA-AM for 60 min as previously described [58]; BAPTA-AM-loaded eggs were washed through five drops of WB/PVA and allowed to recover for 15 min prior to treatment with U0126, ML-7, or the solvent control DMSO. As a control group in these studies of BAPTA-AM-loaded eggs, fertilized eggs were used (i.e., induced to undergo sperm-induced egg activation). In vitro fertilization was performed as described [59] with inseminations of ZP-free eggs performed for 3 h with 100 000 capacitated sperm/ml. For culture of eggs in conditions deficient in extracellular calcium, calcium-deficient WB/PVA was prepared replacing the 4.8 mM lactic acid hemicalcium salt with D,L-lactic acid sodium salt (Sigma) [60]. For certain experiments, eggs were pretreated with the zinc ionophore zinc pyrithione (ZnPT) (Sigma-Aldrich) by culturing eggs in WB/PVA medium containing 10 μM ZnPT for 5 min without an overlay of mineral oil [12, 13, 61]. ZnPT-treated eggs were then washed through five drops of WB/PVA and allowed to recover for 15 min prior to treatment with U0126, ML-7, or the solvent control DMSO.

Measurements of Effective Cortical Tension by Micropipette Aspiration

ZP-free eggs treated with 0.5% DMSO or 50 μM U0126 were subjected to micropipette aspiration, and the effective tension (T_{eff}) calculated as previously described [44].

Immunoblotting

Samples of metaphase II egg proteins were prepared by lysing eggs (90 eggs per sample for pMRLC and MRLC blots, and 35 eggs per sample for pMAPK and MAPK blots) in 10 μl SDS-PAGE sample buffer (65 mM Tris-HCl, 10% glycerol, 3.0% SDS, 0.02% bromophenol blue, 2% β-mercaptoethanol, pH 6.8, supplemented with 100 μM sodium orthovanadate) and heating at 100°C for 10 min. Proteins were separated on 10% (for MAPK and pMAPK) or 12.5% (for MRLC and pMRLC) SDS-PAGE gels, then transferred to Immobilon-P polyvinylidene fluoride membrane (Millipore). Membranes were blocked for 2 h in 10% cold water fish gelatin (Sigma) in 20 mM Tris, 137 mM NaCl, and 0.1% Tween-20 (TBS-T), then incubated overnight at 4°C in primary antibody (diluted in TBS-T with 3% BSA and 0.02% NaN_3). Primary antibodies used here were anti-MRLC (3671; Cell Signaling Technologies) at 125 ng/ml, anti-pMRLC (catalog no. 3672; Cell Signaling Technologies) at 75 ng/ml, anti-MAPK (catalog no. 4695; Cell Signaling Technologies) at 98 ng/ml, and anti-pMAPK (catalog no. 4370; Cell Signaling Technologies) at 0.15 μg/ml. After washing, membranes were then incubated for 2 h at room temperature in goat anti-rabbit immunoglobulin G (IgG) horseradish peroxidase-conjugated secondary antibody (400 ng/ml; Jackson Immunoresearch) diluted in TBS-T with 5% BSA. Immune conjugates were detected using SuperSignal West Pico Chemiluminescent Substrate (Pierce Chemical Company/Thermo Scientific) and x-ray film (Research Products International Corporation). Band intensity was analyzed using ImageJ software (http://rsb.info.nih/gov/ij/), selecting an appropriate exposure time for each blot such that

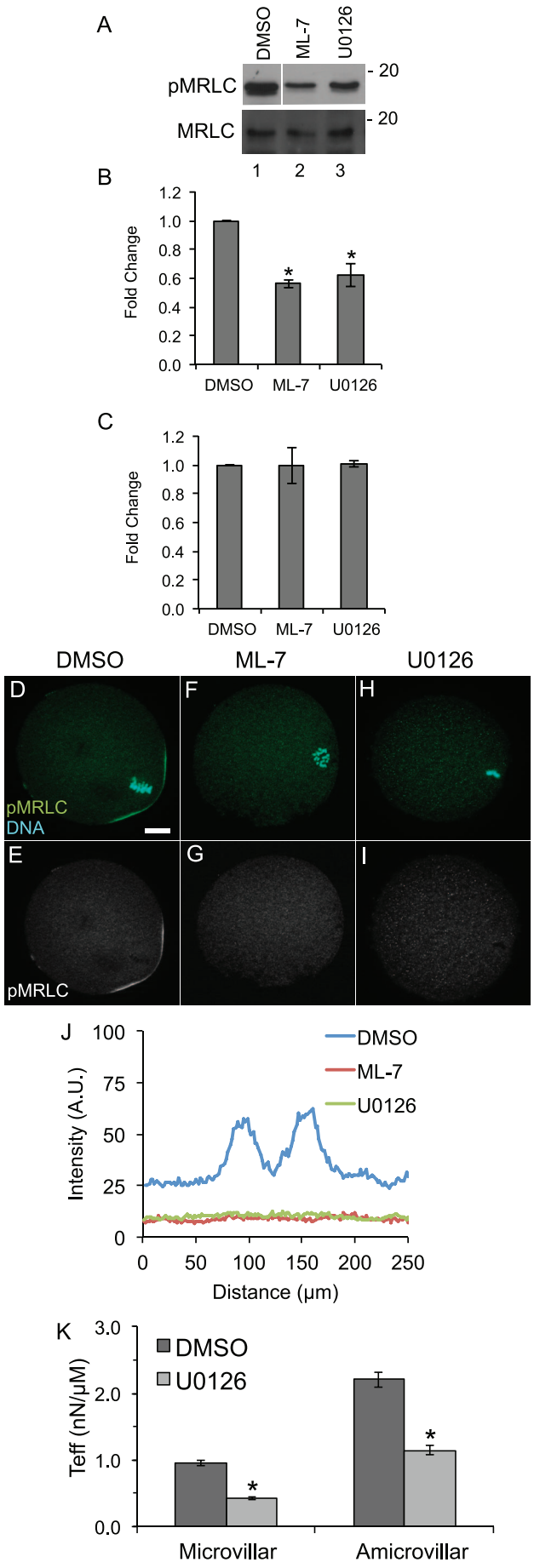

no signals were saturated. The rectangular selection tool was used to select each band, and the peak intensity was determined. The area under each peak was calculated as a measure of band intensity. Band intensities were reported as mean value in arbitrary units ± SEM for each group.

Immunofluorescence and Fluorescence Microscopy

ZP-free eggs were fixed in 4.0% paraformaldehyde (prepared in 130 mM KCl, 25 mM HEPES, 3 mM $MgCl_2$, 0.06% Triton-X, pH 7.4, for 30 min at 37°C), and then permeabilized for 15 min in PBS containing 0.1% Triton X-100 (Sigma), followed by incubations in blocking solution—PBS containing 0.1% BSA, 10% normal goat serum (Invitrogen), and 100 μM sodium orthovanadate—for 60 min, and then primary antibody diluted in blocking solution. Antibodies used here were anti-pMRLC (3675; Cell Signaling Technologies) at 100 ng/ml, the anti-mitotic protein monoclonal antibody MPM-2 [62] (Millipore) at 1.25 μg/ml, anti-β-tubulin rabbit (1799; Epitomics) at 1.35 μg/ml, and anti-α-tubulin monoclonal supernatant diluted 1:5 (clone 12G10; developed by Joseph Frankel and E. Marlo Nelson, obtained from the Developmental Studies Hybridoma Bank developed under the auspices of the National Institute of Child Health and Human Development and maintained by the University of Iowa, Department of Biology). Eggs were washed, then incubated in secondary antibody (7.5 μg/ml goat-anti-mouse IgG-fluorescein isothiocyanate; 7.5 μg/ml donkey-anti-rabbit IgG-Texas Red; Jackson Immunoresearch) or Acti-stain phalloidin-555 (140 nM; Cytoskeleton) for 2 h. Eggs were mounted in Vectashield mounting medium (Vector Laboratories) supplemented with 1.5 μg/ml 4′,6-diamidino-2-phenylindole (DAPI) (Sigma).

Imaging was performed on Zeiss Axio Observer Z1 fluorescence microscope with a Zeiss Axiocam MRm camera, Apotome optical sectioning, and AxioVision software (Carl Zeiss, Inc.). Analysis of the fluorescent intensity of pMRLC and actin signals in the egg cortex was performed using plot profile line scan analysis in ImageJ software (http://rsb.info.nih/gov/ij/), starting the scan around the circumference of the egg at the point of the cortex opposite the maternal DNA and using a line of sufficient width to capture the cortical staining with anti-pMRLC antibody or phalloidin. Analysis of spindle location was performed by viewing each egg from pole to pole. Measurement of the distance of the spindle from the egg periphery was performed on the eggs in

FIG. 1. MAPK3/1 and MLCK inhibition reduces levels of active, phosphorylated myosin regulatory light chain, affects localization of phosphorylated myosin regulatory light chain, and decreases cortical tension in metaphase II eggs. **A**) Representative blots of egg lysates (90 cells per lane treated for 90 min with 0.5% DMSO, lane 1, 15 μM ML-7, lane 2, or 50 μM U0126, lane 3) probed with anti-pMRLC and anti-MRLC. **B** and **C**) Quantification of band intensities of anti-pMRLC levels (**B**) and anti-MRLC levels (**C**). Values were normalized to DMSO-treated eggs. Error bars represent standard errors of the mean. The anti-pMRLC blots were performed 13 times for DMSO-treated eggs, 11 times for ML-7-treated eggs, and eight times for U0126-treated eggs. The difference between levels of pMRLC in ML-7- and U0126-treated eggs is statistically significant as compared to DMSO-treated eggs (Kruskal-Wallis test with Bonferroni-Dunn post hoc testing, $*P < 0.05$). The MRLC blots were repeated four times for all the treatment groups. **D**–**I**) Immunofluorescence shows the localization of anti-pMRLC staining (green, with complementary black-and-white image of this channel in **E**, **G**, and **I**) and DNA (stained with DAPI, in blue) in metaphase II eggs exposed to 0.5% DMSO (**D**, **E**), treated with 15 μM ML-7 (**F**, **G**), or with 50 μM U0216 (**H**, **I**). Bar in **D** = 10 μm. **J**) Line-scan analysis around the circumference of the cortical region to assess relative intensities of the pMRLC cortical signal in DMSO-, ML-7-, and U0126-treated eggs. This graph shows pooled data from 23 DMSO-treated metaphase II eggs (blue line), 12 ML-7-treated eggs (red line; four metaphase II, six metaphase II drifted spindle, two anaphase II), and 18 U0126-treated eggs (green line; eight metaphase II, six metaphase II drifted spindle, and four anaphase II); see also Supplemental Figure S1 for data on individual eggs. In DMSO-treated eggs, the two peaks in these scans coincide with pMRLC at the two boundaries of the amicrovillar domain. The line scans of ML-7- and U0126- treated eggs do not show these peaks. **K**) Effective tension (T_{eff}, in nN/μm) on the microvillar and amicrovillar domains of DMSO-treated eggs (dark gray) and U0126-treated eggs (light gray) as measured by micropipette aspiration. Error bars represent standard errors of the mean. This decrease in effective tension is statistically significant (Mann-Whitney *U*-test, $*P < 0.05$). Numbers of eggs analyzed: DMSO-treated microvillar domain, 36; U0126-treated microvillar domain, 79; DMSO-treated amicrovillar domain, 18; and U0126-treated amicrovillar domain, seven.

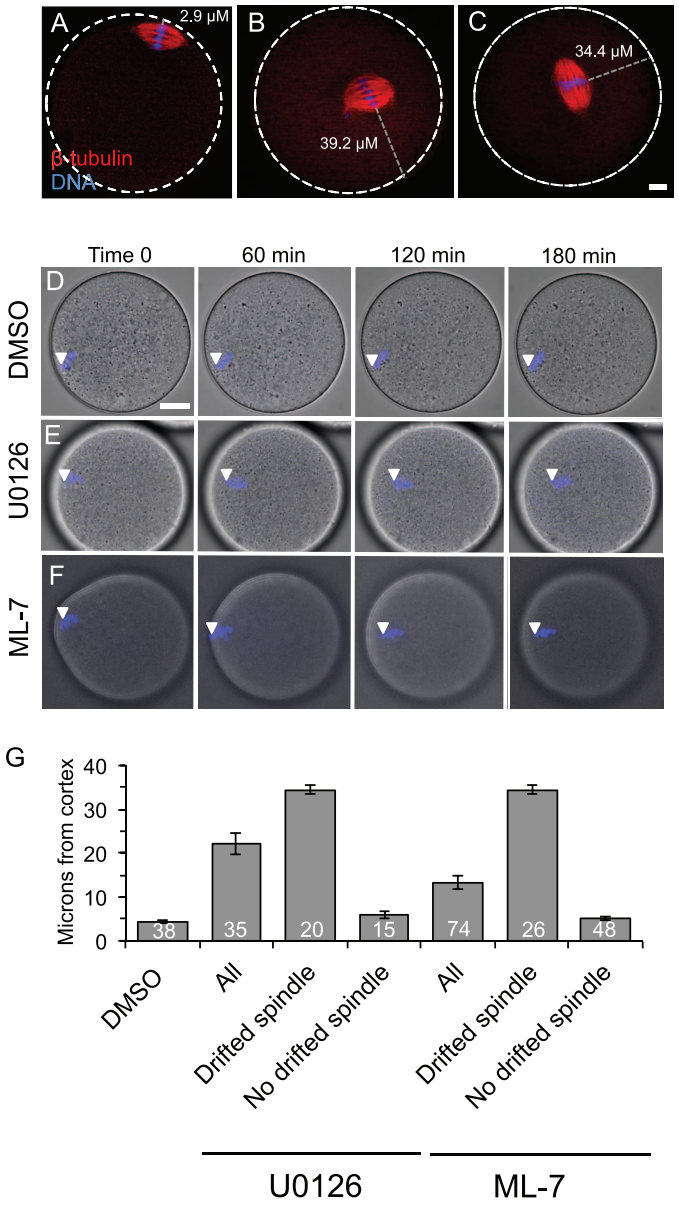

FIG. 2. Spindle localization in U0126- and ML-7-treated metaphase II eggs. **A**–**C**) Fluorescence images show the localization of the metaphase II spindle in eggs stained with anti-β-tubulin (red) and DAPI to stain the maternal DNA (blue). White dotted lines show the perimeter of the egg. **A** shows a control egg with normal spindle localization. **B** and **C** show representative U0126- and ML-7-treated eggs in which the metaphase II spindle has drifted away from the cortex. The gray dotted line indicates how spindle distance was measured (in μm) using the point of the maternal DNA on the metaphase plate closest to the egg periphery as the start point, and the egg perimeter as the end point. Bar in **C** = 10 μm for **A**–**C**. **D**–**F**) Time-lapse microscopy of DAPI-loaded eggs over time, with eggs treated with DMSO (**D**), 50 μM U0126 (**E**), or 15 μM ML-7 (**F**). **D** and **E** show single optical sections (because the spindle was moving within this plane), and **F** is a three-dimensional maximum intensity projection (MIP) image from multiple optical sections. White arrowheads indicate the localization of the DAPI-stained maternal DNA. Bar in **D** = 17 μm for **D**–**F**. **G**) Average spindle-to-cortex distances (in μm) in DMSO-, U0126-, and ML-7-treated eggs. The U0126- and ML-7-treated eggs are further separated into the subgroup of eggs with drifted spindles (i.e., cortex-to-DNA distance greater than 12 μm) and the subgroup of eggs with no drifted spindle (i.e., cortex-to-DNA distance less than 12 μm). Control DMSO-treated eggs had spindles that were a maximum of 10.5 μm from the cortex (mean 5.2 ± 0.4 μm). See text for additional details.

which the spindle was observed to be within ~6 μm of the equator, with images taken in the focal plane of the equator of the egg. Using AxioVision software, the spindle-to-cortex distance was measured using the point of the maternal DNA on the metaphase plate closest to the egg periphery as the start point, and the egg perimeter as the end point (see Fig. 2A–C). An egg was classified as having a MII drifted spindle if the DNA was aligned along the metaphase II plate and the spindle was more than 12 μm from the cortex. The intensity of MPM-2 staining was quantified using ImageJ. Images used for quantification of cytosolic MPM-2 signal were taken near the equator of the egg and avoiding the metaphase II spindle (because the metaphase II spindle was labeled by MPM-2 staining [63]). A region of interest (ROI) covering the egg was defined, and the fluorescence signal within this egg ROI was calculated (using the integrated density measurement in ImageJ, a product of the ROI area and ROI mean gray value). Background fluorescence signal values were obtained for each image from an identically sized ROI taken outside of the egg; this background fluorescence signal value was calculated as the mean fluorescence of the background ROI multiplied by the area of the ROI. The corrected total cell fluorescence value for each egg was calculated as the integrated density of the egg ROI minus the background fluorescence signal value.

Live-Cell Time-Lapse Imaging

ZP-free eggs were loaded with DAPI by culturing in WB/PVA medium containing 1 μg/ml DAPI for 90 min, followed by washing through three drops of WB/PVA. DAPI-loaded eggs were placed in 10 μl drops of WB/PVA containing either 0.5% DMSO, 15 μM ML-7, or 50 μM U0126 in poly-L-lysine-coated MatTek 35 mm glass bottom culture dishes covered with mineral oil. Imaging was performed with cells at 37°C in 5% CO_2 in an environmental control unit on a Zeiss Observer Z1 fluorescence microscope with a Zeiss Axiocam MRm camera, Apotome optical sectioning, and AxioVision software (Carl Zeiss, Inc.). Images were acquired using a Zeiss EC Plan-Neofluar 40× objective (numerical aperture 1.3) every 5 min for 3 h, collecting z-stacks of approximately 10 optical sections per egg.

Statistical Analyses

Analyses were performed using StatView 5.0 (SAS Institute). A *P*-value less than 0.05 was considered significant. Error bars in figures represent the standard error of the mean. Kruskal-Wallis tests with Bonferroni-Dunn post hoc testing were used to analyze immunoblot band intensity data. A one-way analysis of variance (ANOVA) with Fisher's projected least significant difference post hoc test was used to analyze MPM-2 fluorescent intensities. Chi-squared tests were used to compare rates of spontaneous activation. The nonparametric Mann-Whitney *U*-test was used to test for statistical significance in effective cortical tension measurements.

RESULTS

Inhibition of the MAPK Pathway in Eggs Contributes to Reduced Function of Myosin-II

As noted in the *Introduction,* MAPK3/1 has multiple functions in metaphase II eggs and has been implicated as functioning upstream of MLCK [41, 42, 48]. We set out to examine the connection between MAPK signaling and myosin-II function in eggs and to ascertain the potential implications of this pathway for metaphase II arrest. U0126 was used to inhibit the MAPK pathway through inhibition of the MAPK-activating kinases MEK1 and MEK2. Studies here used a U0126 dose of 50 μM, based on previous studies of U0126-induced parthenogenetic egg activation and the finding that doses of 100 μM and higher became cytotoxic to eggs with prolonged cultured time [26]. ML-7 was used to inhibit MLCK using a dose of 15 μM based on past work [44, 49]. Multiple other studies have used U0126 or ML-7 on mouse oocytes as well [27, 37, 38, 40, 47, 48, 50, 51, 55, 64].

We assessed the effects of these drug treatments on the myosin-II-based cytoskeleton in three ways. First, immunoblotting revealed U0126- and ML-7-treated eggs had ~50% the levels of active, phosphorylated myosin regulatory light chain (pMRLC) compared to control eggs treated with the solvent DMSO (Fig. 1, A and B). Control, U0126-treated, and

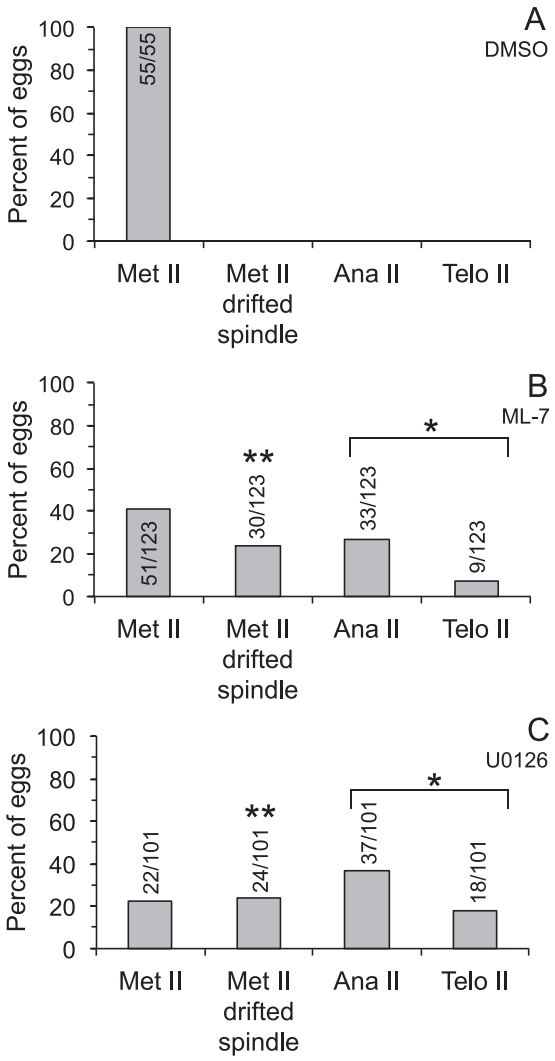

FIG. 3. Effects of U0126 or ML-7 treatment in metaphase II eggs. Metaphase II eggs were treated with 0.5% DMSO (**A**), 15 μM ML-7 (**B**), or 50 μM U0126 (**C**) for 3 h, then fixed and stained with DAPI to label DNA, anti-β-tubulin to label the meiotic spindle, and the monoclonal antibody MPM-2 to label mitotic phosphoproteins (analysis shown in Fig. 5). Eggs were classified as metaphase II (Met II; normal metaphase II spindle morphology and cortical localization), Met II drifted spindle (i.e., the DNA was aligned along the metaphase II plate and the spindle was greater than 12 μm from the cortex; shown in Fig. 2), anaphase II, or telophase II (Ana II and Telo II, respectively, i.e., progressing out of metaphase II arrest). Numbers in or above bars indicates numbers of eggs analyzed. The extent of progression out of metaphase II arrest (combined numbers of eggs in anaphase II and telophase II states) in U0126- and ML-7-treated eggs is statistically significant as compared to DMSO-treated eggs (chi-square analysis, $*P < 0.0001$). The extent of drifted spindle incidences in U0126- and ML-7-treated eggs is statistically significant as compared to DMSO-treated eggs (chi-square analysis, $**P < 0.0001$).

ML-7-treated eggs had comparable amounts of total MRLC (Fig. 1, A and C). Control experiments with anti-MAPK3/1 antibodies and anti-phosphoMAPK3/1 (pMAPK3/1) antibodies verified that ML-7 treatment of metaphase II eggs did not alter MAPK3/1 protein levels or phosphorylation (Supplemental Fig. S1A–C; Supplemental Data are available online at www.biolreprod.org), and that U0126 treatment reduced phospho-MAPK3/1 protein levels (data not shown). Second, immunofluorescence and image analysis revealed that U0126 or ML-7 treatment affected pMRLC localization in metaphase II eggs. Phosphorylated MRLC was detected in control metaphase II eggs in the boundaries of the amicrovillar domain overlying the meiotic spindle (Fig. 1, D, E, and J). However, in U0126- and ML-7-treated eggs, this pMRLC signal was greatly reduced (Fig. 1F–J). Third, as an additional assessment of actomyosin function in U0126-treated eggs, we examined cortical tension using micropipette aspiration, providing insight into contractility of the cortical cytoskeleton [44, 65, 66]. Our previous work showed that treatment of eggs with 15 μM ML-7 reduced effective tension (T_{eff}) in metaphase II eggs by ~50% in the amicrovillar domain (over the maternal DNA) and microvillar domain (the domain away from the maternal DNA and to which sperm bind and fuse) [44]. U0126-treated metaphase II eggs had similar decreased effective cortical tension in the amicrovillar and microvillar domains (Fig. 1K); U0126 treatment resulted in effective cortical tension being reduced to 56% of control levels in the microvillar domain and to 48% of control levels in the amicrovillar domain. Taken together, these data suggest that inhibition of the MAPK pathway in metaphase II eggs contributed to dysfunction of nonmuscle myosin-II, in a fashion that has similarities to inhibition of MLCK.

Inhibition of MEK/12 with U0126 or of MLCK with ML-7 Causes Loss of Spindle Localization Adjacent to the Cortex in a Subset of Drug-Treated Metaphase II Eggs

Eggs were treated with the solvent control DMSO, 50 μM U0126, or 15 μM ML-7, and then imaged by time-lapse microscopy or fixed after 3 h treatment and stained to label the DNA and meiotic spindle as well as mitotic phospho-proteins (addressed in more detail below). In eggs exposed to the solvent DMSO, the maternal DNA was localized directly beneath the cortex (Fig. 2, A and D). However, in a subset of U0126- and ML-7-treated eggs, the metaphase II spindle drifted away from its normal cortical location (Fig. 2, B, C, E, and F; identified as MII drifted spindle in Figs. 3, 4, 7, and Supplemental Figs. S2 and S3), in agreement with another study of MEK inhibition in eggs [37]. DMSO-treated eggs had spindles that were a maximum of 10.5 μm from the cortex (mean 5.2 ± 0.4 μm; Fig. 2G). U0126-treated eggs had spindles that were an average of 20.2 ± 2.1 μm from the cortex (column labeled as all in Fig. 2G), although U0126-treated eggs fell into two distinct groups: eggs with spindles that were a similar distance as in DMSO-treated eggs (average 6.4 ± 0.8 μm, range 1.8–11.5 μm, and labeled as no drifted spindle in Fig. 2G) and eggs with spindles that were significantly farther from the cortex (average 32.9 ± 1.4 μm, range 23.5–40.5 μm, and labeled as drifted spindle in Fig. 2G). A similar trend was observed in ML-7-treated eggs. ML-7-treated eggs had spindles that were an average of 13.9 ± 1.4 μm from the cortex (Fig. 2G), with a subset of eggs with spindles that were similar to DMSO-treated eggs (average 5.4 ± 0.5 μm, range 0.8–11.3 μm), and the remaining eggs categorized as having drifted spindles (average 28.3 ± 1.6 μm, range 15.6–46.4 μm). This drifted spindle phenomenon, defined as the spindle being more than 12 μm from the cortex, was observed in 24% of ML-7-treated eggs and 24% of U0126-treated eggs after 3 h of drug treatment (Fig. 3, B and C), whereas none of the DMSO control eggs had a metaphase II spindle that drifted from its cortical location (Fig. 3A). Complementary studies assessed the time dependence of this spindle drift, examining eggs fixed at 1.5 or 8 h after the start of drug treatment (Supplemental Figs. S2 and S3). At the 1.5 h time point, 18/52 ML-7-treated eggs and 4/28 of U0126-treated eggs showed signs of spindle drift (Supplemental Fig. S2). At 8 h, 12/45 ML-7-treated eggs and 5/120 U0126-treated eggs showed signs of spindle drift

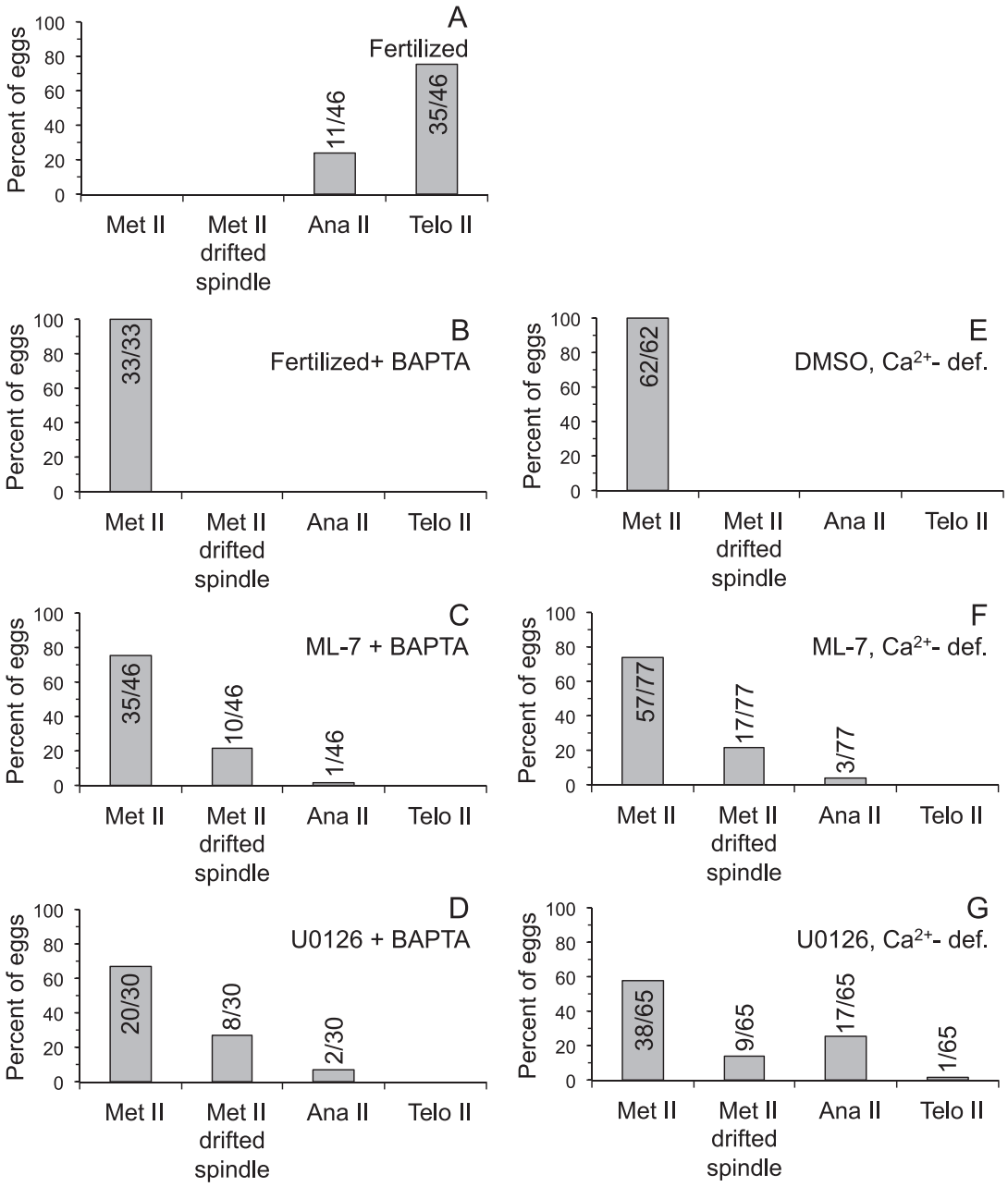

H

Drug	Ca^{2+} Manipulation	# eggs exiting from MII arrest/total eggs: Drug alone	# eggs exiting from MII arrest/total eggs: Drug + Ca^{2+} Manipulation
ML-7	BAPTA-AM	31% (14/45)	2% (1/46)*
	Ca^{2+}-deficient	36% (28/78)	4% (3/77)*
U0126	BAPTA-AM	55% (30/55)	7% (2/30)*
	Ca^{2+}-deficient	54% (25/46)	28% (18/65)*

FIG. 4. Calcium dependence of U0126- and ML-7-induced parthenogenetic exit from metaphase II arrest. **A**) Fertilized: shows control eggs, not loaded with BAPTA-AM and inseminated. For **B**–**D**, eggs were preloaded with 5 μM of the calcium chelator BAPTA-AM and then inseminated (**B**, fertilized + BAPTA-AM) or treated with 15 μM ML-7 (**C**) or 50 μM U0126 (**D**) for 3 h. For **E**–**G**, eggs were cultured in Ca^{2+}-deficient medium and treated with 0.5% DMSO (**E**), 15 μM ML-7 (**F**), or 50 μM U0126 (**G**) for 3 h. After the 3 h treatment or insemination, eggs were fixed and stained with DAPI to label DNA, anti-β-tubulin to label the meiotic spindle, and MPM-2 to label mitotic phosphoproteins (analysis shown in Fig. 5). Eggs were classified as in Figure 3: metaphase II (Met II; normal metaphase II spindle morphology and cortical localization), Met II drifted spindle (i.e., the DNA was aligned along the metaphase II plate and the spindle was greater than 12 μm from the cortex; shown in Fig. 2), anaphase II, or telophase II (Ana II and Telo II, respectively,

(Supplemental Fig. S3). A likely explanation for the smaller number of U0126-treated eggs having mislocalized spindles is that the majority of U0126-treated eggs at this 8 h time point exited from metaphase II arrest, in agreement with other work [26, 37] and addressed below.

Inhibition of MEK1/2 with U0126 or of MLCK with ML-7 Causes Spontaneous Parthenogenetic Exit from Metaphase II Arrest in a Subset of Drug-Treated Eggs

A second phenotype detected in U0126-treated eggs is exit from metaphase II arrest [26]. In our studies here, 54% of U0126-treated eggs were in anaphase or telophase of meiosis II after 3 h after the start of drug treatment (Fig. 3C). Interestingly, we also observed exit from metaphase II arrest in 34% of the ML-7-treated eggs (Fig. 3B). Further studies assessed the time dependence of this exit from metaphase II arrest. At 1.5 h after the start of drug treatment, none of the DMSO control eggs had exited from metaphase II arrest, whereas 10% (5/52) of ML-7-treated eggs and 29% (8/28) of U0126-treated eggs exited from metaphase II arrest (Supplemental Fig. S2). At 8 h after the start of drug treatment, none of the DMSO control eggs had exited from metaphase II arrest, whereas 58% (26/45) of ML-7-treated eggs and 93% (112/120) of U0126-treated eggs exited from metaphase II arrest (Supplemental Fig. S3). The majority of the eggs that had exited from metaphase II arrest at this 8 h time point had progressed to a pronuclear-like stage (Supplemental Fig. S3), in agreement with previous work [26, 37].

U0126-Induced or ML-7-Induced Parthenogenetic Exit from Metaphase II Arrest Is Dependent on Calcium

Fertilization-induced exit from metaphase II arrest is triggered by an increase in cytosolic calcium (reviewed in [31]). Additionally, extracellular calcium is required for fertilization-induced meiosis II completion in mouse and for increased intracellular Ca^{2+} and egg activation in *Drosophila* induced in vitro by ovulation-mimicking stimuli [67–69], suggesting that calcium influx is involved in these egg activation events. Therefore, we tested the hypotheses that 1) U0126- or ML-7-induced exit from metaphase II arrest was dependent on calcium in the egg cytoplasm, and 2) U0126- or ML-7-induced exit from metaphase II arrest was dependent on extracellular calcium.

Experiments testing whether intracellular calcium played a role in U0126- or ML-7-induced egg activation used eggs pretreated with the calcium chelator BAPTA-AM followed by treatment with U0126 or ML-7. We used a dose of 5 μM BAPTA-AM because this prevents any detectable increase in cytosolic calcium following fertilization or treatment with conventional parthenogenetic stimuli, such as the calcium ionophore A23187 or $SrCl_2$ [58, 70]. As a control here, we confirmed that fertilized BAPTA-AM-loaded eggs remained in metaphase II (Fig. 4B) [70]. Preloading eggs with BAPTA-AM prior to treatment with U0126 or ML-7 dramatically reduced the extent of exit from metaphase II arrest at 3 h after the start of drug treatment. Only 2% of ML-7-treated eggs and 7% of U0126-treated eggs that had been preloaded with BAPTA-AM exited from metaphase II arrest, versus 31% of ML-7-treated eggs and 55% of U0126-treated eggs that were not treated with BAPTA-AM (Fig. 4, C and D); Figure 4H summarizes the effects on metaphase II exit with U0126 or ML-7 (drug alone column, which are part of the data in Fig. 3) as compared to BAPTA-AM loading prior to drug treatment (i.e., drug + Ca^{2+} manipulation column). It is worth noting that the drift of the metaphase II spindle from its normal cortical position occurred to comparable extents in U0126- and ML-7-treated eggs with and without BAPTA-AM (Figs. 3 and 4), suggesting this spindle drift phenomenon induced by MAPK3/1 or MLCK inhibition is not dependent on intracellular calcium.

Experiments testing whether extracellular calcium played a role in U0126- or ML-7-induced egg activation used eggs cultured in Ca^{2+}-deficient medium. We observed that a reduced extent of U0126- or ML-7-induced exit from metaphase II arrest occurred in eggs cultured in Ca^{2+}-deficient medium as compared to eggs cultured in medium containing Ca^{2+} (Fig. 4F–H). Following 3 h of inhibitor treatment in Ca^{2+}-deficient medium, only 4% of ML-7-treated eggs exited from metaphase II arrest (Fig. 4F) as compared to 36% of ML-7-treated eggs cultured in Ca^{2+}-containing medium (Fig. 4H); Figure 4H summarizes the effects on metaphase II exit with drug treatment in Ca^{2+}-containing medium (drug alone column, which is part of the data in Fig. 3) as compared to drug treatment in Ca^{2+}-deficient medium (drug+Ca^{2+} manipulation column). In eggs treated with U0126, 28% of eggs in Ca^{2+}-deficient medium underwent parthenogenetic activation as compared to 54% of U0126-treated eggs cultured in parallel in Ca^{2+}-containing medium (Fig. 4H). DMSO-treated control eggs in Ca^{2+}-deficient medium remained at metaphase II (Fig. 4E). To assess the time dependence of these effects on metaphase II exit, eggs were examined at 1.5 h or 8 h after the start of drug treatment in eggs preloaded with BAPTA-AM or cultured in Ca^{2+}-deficient medium (Supplemental Figs. S2 and S3). There was a very modest extent of exit from metaphase II arrest after 1.5 h treatment with ML-7 or U0126 in Ca^{2+}-deficient medium (1/57 eggs and 3/30 eggs, respectively; Supplemental Fig. S2). The extent of exit from metaphase II arrest at the 8 h time point was roughly comparable in Ca^{2+}-deficient medium and Ca^{2+}-containing medium and with and without BAPTA-AM loading prior to ML-7 or U0126 treatment (Supplemental Fig. S3), suggesting that parthenogenetic egg activation in response to protracted inhibition of MAPK or MLCK is less dependent on extracellular calcium than is parthenogenesis after 1.5–3 h of ML-7 or U0126 treatment.

To complement the assessment of the maternal DNA and meiotic spindle (i.e., metaphase, anaphase, or telophase), we examined M-phase status by quantifying mitotic phosphoepitopes detected in immunofluorescence with the monoclonal

i.e., progressing out of metaphase II arrest). Numbers in or above the bar indicates numbers of eggs analyzed. **H**) Summary of the effects of ML-7 and U-126 on metaphase II exit, providing data for control eggs (drug alone refers to ML-7 or U0126 in Ca^{2+}-containing medium) compared to eggs treated with drug + Ca^{2+} manipulation (referring to ML-7 or U0126 combined with BAPTA-AM or culture in Ca^{2+}-deficient medium). The data in the "drug alone" column are part of what is shown in Figure 3, with the data here from the specific experiments using U0126 or ML-7 treatment cultured in parallel in experiments with the indicated Ca^{2+} manipulation (i.e., either BAPTA-AM treatment prior to drug treatment or drug treatment in Ca^{2+}-deficient medium). The extent of progression out of metaphase II arrest (combined numbers of eggs in anaphase II and telophase II states) in ML-7-treated eggs preloaded with BAPTA-AM or cultured in Ca^{2+}-deficient medium is statistically significant as compared to ML-7-treated eggs without the indicated Ca^{2+} manipulation (chi-square analysis, $^*P < 0.005$). The extent of progression out of metaphase II arrest in U0126-treated-eggs preloaded with BAPTA-AM is statistically significant as compared to U0126-treated eggs without the indicated Ca^{2+} manipulation (chi-square analysis, $^*P < 0.005$).

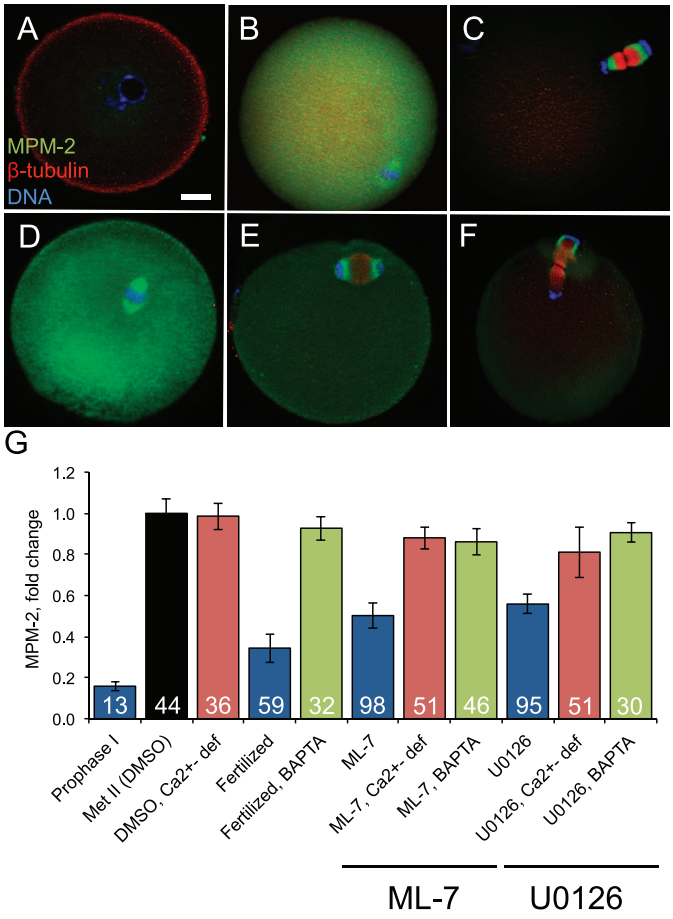

FIG. 5. Analysis of M-phase phospho-protein levels detected by MPM-2 staining. The monoclonal antibody MPM-2, which reacts with M-phase-specific phospho-epitopes, was used to assess M-phase status in individual eggs. **A**–**F**) Representative eggs that were stained with MPM-2 (green), anti-β-tubulin (red), and DAPI (blue) are shown. **A**–**C** show control cells at prophase I, metaphase II, and embryonic interphase (embryos fixed at 3 h postinsemination). Prophase I oocytes have low CDK1 activity and thus a low MPM-2 signal. Metaphase II arrested eggs have high CDK1 activity and thus a high MPM-2 signal. Early embryos have low CDK1 activity and low MPM-2 signal. **D**–**F** show representative eggs treated with 15 μM ML-7 or 50 μM U0126. **D** shows a representative egg with a metaphase II spindle that has drifted away from the cortex. **E** and **F** show representative eggs that have progressed to anaphase II and telophase II following inhibitor treatment. Bar in **A** = 10 μm for **A**–**F**. **G**) Quantification of the intensity of MPM-2 signals in eggs in the different experimental treatment groups. Numbers in bars indicate the numbers of eggs analyzed in each experimental group. Error bars represent standard error of the mean. Metaphase II DMSO-treated eggs are shown in the black bar. Prophase I oocytes, fertilized eggs, and ML-7-treated and U0126-treated eggs are shown in blue. The average MPM-2 signal intensities in ML-7- and U0126-treated eggs were statistically significantly different ($P < 0.05$; ANOVA with Fisher's protected least significant different post hoc testing) compared to DMSO-treated eggs (black bar). Eggs in which intracellular Ca^{2+} was chelated by pretreating with BAPTA-AM are shown in green combined with either fertilization (labeled fertilized: these eggs do not exit from metaphase II arrest and thus have high MPM-2 signals) or with ML-7 or U0126 treatment. Eggs that were treated with DMSO, ML-7, or U0126 in Ca^{2+}-deficient medium are shown in in red. The average MPM-2 signal intensities for ML-7- and U0126-treated eggs without BAPTA-AM and in Ca^{2+}-containing medium (blue bars) were statistically significantly different as compared to the comparable drug treatment group with either BAPTA-AM loading (green bars) or when drug treatment occurred in Ca^{2+}-deficient medium (red bars) ($P < 0.05$; ANOVA with Fisher's protected least significant difference post hoc testing).

antibody MPM-2 [62]. The MPM-2 signal was quantified in individual eggs in each experimental group and normalized to control metaphase II eggs, defined as 1 (black bar, labeled as Met II [DMSO] in Fig. 5G). Metaphase II eggs have high CDK1 activity and thus had strong MPM-2 signals (Fig. 5, B and G) [63]. Other controls were prophase I oocytes and early embryos fixed at 3 h after insemination. Prophase I oocytes, with low CDK1 activity, had very faint MPM-2 signals (Fig. 5, A and G, blue bar). Early embryos, with declining CDK1 activity with exit from metaphase II arrest, had decreased MPM-2 signals (Fig. 5, C and G, blue bar). Representative eggs treated with ML-7 or U0126 are also shown, with a metaphase II spindle that has drifted from the cortex (Fig. 5D) or that had progressed to anaphase II or telophase II following 3 h of inhibitor treatment (Fig. 5, E and F). MPM-2 levels in eggs treated with U0126 or ML-7 were ~55% the MPM-2 levels detected in control metaphase II eggs ($P < 0.05$, blue bars). In contrast, U0126- and ML-7-treated eggs that were either pretreated with the calcium chelator BAPTA-AM (Fig. 5G, green bars) or cultured in Ca^{2+} deficient medium (Fig. 5G, red bars) had MPM-2 levels that were similar to MPM-2 levels in control metaphase II eggs.

Treatment with a Zinc Ionophore Rescues U0126-Induced or ML-7-Induced Exit from Metaphase II Arrest

The data above suggest that U0126- or ML-7-induced parthenogenetic activation and a loss of M-phase phospho-proteins were dependent on calcium. As noted in the *Introduction,* another contributor to metaphase II arrest and exit from this arrest is zinc; zinc appears to act on EMI2, a zinc-binding protein that is an inhibitor of the APC [11–13, 29]. Decreased cytosolic zinc is important for exit from metaphase II arrest because treatment of eggs with the zinc ionophore ZnPT prior to $SrCl_2$-induced activation significantly reduces the extent of progression to pronuclear stage, indicative of mitotic interphase [12, 13]. We therefore tested the hypothesis that U0126- and ML-7-induced parthenogenesis could be rescued by manipulating zinc levels in the egg. Eggs were hyperloaded with zinc by treating with ZnPT [12, 13] prior to treating the eggs with U0126 or ML-7.

The effects of these treatments on the egg actomyosin cytoskeleton were assessed. DMSO-treated eggs have F-actin enriched in the amicrovillar domain over the metaphase II spindle, with pMRLC at the boundary of the amicrovillar domain (Fig. 6A and line scan analysis of these signals in Fig. 6, D and G). On the other hand, ML-7-treated eggs (Fig. 6, B, E, and H) and U0126-treated eggs (Fig. 6, C, F, and I) do not show this enrichment of actin and pMRLC in the amicrovillar domain. Similar data were obtained for eggs treated with ZnPT prior to culture in DMSO, U0126, or ML-7, indicating that the ZnPT treatment did not rescue normal actin or pMRLC localization in the ML-7- or U0126-treated eggs (Fig. 6, J–R). In addition, we verified that effective cortical tension of ZnPT-treated eggs was similar compared to untreated control eggs (microvillar domains: 0.94 ± 0.04 nN/μm for control, 0.96 ± 0.03 nN/μm for ZnPT-treated; amicrovillar domains, 2.22 ± 0.10 nN/μm for control, 2.29 ± 0.11 nN/μm for ZnPT-treated; n = 10 eggs for each experimental group). These data showed that the ZnPT treatment used here did not affect cortical tension in eggs.

ZnPT treatment reduced parthenogenesis in ML-7- and U0126-treated eggs. Only 3% of U0126+ZnPT-treated eggs exited from metaphase II arrest compared to 88% of U0126-treated eggs exiting from metaphase II arrest ($P < 0.05$; Fig. 7, C and F). This trend held for the ML-7-treated eggs, with 5%

of ML-7+ZnPT-treated eggs exited from metaphase II arrest compared to 21% of ML-7-treated eggs exiting from metaphase II arrest ($P = 0.06$; Fig. 7, B and E). We also assessed M-phase status through analysis of MPM-2 signal intensities (see also Fig. 5). Eggs treated with ML-7 or U0126 had reduced MPM-2 levels as compared to control metaphase II eggs (76% and 49%, respectively, $P < 0.05$; Fig. 7G). On the other hand, eggs pretreated with ZnPT prior to treatment with ML-7 or U0126 had MPM-2 levels that were similar to control metaphase II eggs, consistent with zinc hyperloading via ZnPT treatment suppressing ML-7- or U0126-induced parthenogenesis.

DISCUSSION

This work presents evidence that the MAPK3/1 pathway affects myosin-II-dependent functions in metaphase II mouse eggs. U0126-treated eggs have reduced levels of pMRLC as compared to control eggs and have reduced effective cortical tension. This U0126-induced reduction in cortical tension is similar to what we observe in ML-7-treated eggs [44], which have similarly reduced pMRLC levels (Fig. 1). Interestingly, MAPK3/1 activity also can affect cortical tension at a different time in meiosis, albeit by what may be a different mechanism. In meiosis I, MAPK3/1 activity increases after germinal vesicle breakdown, activated by Mos [6, 71, 72]. Wild-type oocytes undergo a decrease in cortical tension at 6 h after germinal vesicle breakdown, whereas *mos*-null oocytes do not show this decrease [40]. These cortical tension changes in meiosis I are associated with phosphorylation of the MAPK3/1 substrate WAVE2, which in turn could lead to activation of the actin-related protein-2/3 (ARP2/3) complex and changes in cortical actomyosin (i.e., thickening of cortical actin and loss of cortical myosin-II heavy chain MYH9) [40].

Two effects were observed here in eggs with reduced MAPK3/1 or MLCK activity. The first was a loss of cortical anchoring of the metaphase II spindle. This had been reported for U0126-treated eggs [37], and we show here that this loss of spindle anchoring also occurs in ML-7 treated eggs. There are other reports of loss of normal spindle localization. Expression of a dominant-negative version of the GTPase Rac1 in metaphase II eggs induces either a loss of cortical anchoring of one spindle pole or a gradual loss of cortical spindle localization [73]. Treatment of metaphase II eggs with the ARP2/3 complex inhibitor CK-666 induces a rapid loss of cortical spindle localization, evident within a few minutes of exposing eggs to CK-666 [74], whereas this rapid loss of spindle localization was not detected in eggs treated with blebbistatin, an inhibitor of the myosin-II ATPase [74]. As noted above and previously, our attempts to disrupt myosin-II with blebbistatin unfortunately have not been successful [44]. U0126- and ML-7-induced spindle drift is not detected in the time frame used in the studies of CK-666 and blebbistatin, and instead occurs substantially more slowly. These data suggest that what was observed here with U0126 and ML-7 differs from CK-666-induced spindle drift, which presumably has an underlying cause involving loss of actin nucleation mediated by the ARP2/3 complex.

The second effect observed in eggs with reduced MAPK3/1 or MLCK activity is parthenogenetic exit from metaphase II arrest. We show here that U0126- and ML-7-induced exit from metaphase II is dependent on intracellular calcium because the extent of parthenogenetic activation induced by U0126 or ML-7 treatment is dramatically reduced in eggs loaded with the calcium chelator BAPTA-AM. Our data further suggest that extracellular calcium is important for this U0126- or ML-7-induced parthenogenesis. This agrees with studies showing that external calcium is required for egg activation in *Drosophila* and for completion of meiosis II in mouse [67, 68]. Excitingly, we find that parthenogenetic exit from metaphase II arrest induced by U0126 or ML-7 treatment is rescued by treating eggs with a zinc ionophore, further demonstrating the importance of zinc in the maintenance of metaphase II arrest [11–13, 29].

The data here are consistent with the model that an influx of Ca^{2+} and an efflux of Zn^{2+} are important for egg activation [12, 31, 67–69]. Although mechanisms of postfertilization Zn^{2+} loss and Ca^{2+} entry are not fully understood, there are several possible ways by which Ca^{2+} influx and/or Zn^{2+} efflux could be affected in U0126- or ML-7-treated eggs, particularly with cytoskeletal disruptions being downstream effects of MAPK3/1 and MLCK inhibition. Zinc loss from fertilized eggs has been speculated to occur by exocytosis [12, 75], which could be affected by disruptions of the actomyosin cytoskeleton [49, 76–78]. An additional contribution to zinc loss could be via zinc transporters [79–81], and calcium influx in eggs is likely channel-mediated. There are at least two possible, not mutually exclusive, ways by which cytoskeletal function could affect channel/transporter activity: 1) actomyosin-facilitated trafficking that localizes ion channels/transporters in the plasma membrane (e.g., [82–85]) and 2) actomyosin-based effects on mechanosensitive channels [86–88]. With decreased cortical tension associated with MAPK3/1 or MLCK inhibition, it is tempting to speculate that a mechanosensitive channel(s) underlies U0126- or ML-7-induced parthenogenesis. The nonselective, Ca^{2+}-permeant transient receptor potential (TRP) channels are intriguing candidates to be these mechanosensitive channels [69, 84, 86, 88]. However, little is known about TRP channels in mammalian eggs; only TRPV3 is thus far characterized in mouse eggs, and its role in normal egg activation is unclear (but TRPV3 does appears to mediate Sr^{2+} influx in $SrCl_2$-induced artificial egg activation) [89]. It is very likely that multiple channels could mediate Ca^{2+} influx into eggs. Overall, the regulation of ion homeostasis in normal eggs is far from fully understood, but future studies in these

FIG. 6. Effects of U0126 or ML-7 treatment ± zinc ionophore on actin and pMRLC. Eggs were treated with DMSO, ML-7, or U0126 for 3 h, or were pretreated with 10 μM zinc pyrithione (ZnPT) for 5 min, then with DMSO, ML-7, or U0126 for 3 h prior to localization of pMRLC and actin. Numbers of eggs analyzed: DMSO, nine; ML-7, nine; U0126, 17; DMSO+ZnPT, seven; ML-7+ZnPT, 14; and U0126, 13. Representative fluorescence images of pMRLC (green), actin (red), and DNA (blue) are shown for eggs treated with DMSO (**A**), ML-7 (**B**), or U0126 (**C**), DMSO+ZnPT (**J**), ML-7+ZnPT (**K**), or U0126+ZnPT (**L**). **D**–**F** and **M**–**O** are data from line scans around the circumference of the egg (starting at the point opposite the DNA) of cortical actin signals in **A**–**C**. The peaks in **D** and **M** correspond to the cortical actin cap overlying the DNA in **A** and **J**, respectively. The line scans in **E**, **F**, **N**, and **O** have no distinct peak, coinciding with the loss of the actin cap overlying the DNA following inhibitor treatment in **B**, **C**, **K**, and **L**, respectively. **G**–**I** and **P**–**R** are line scans of the cortical pMRLC fluorescence in **A**–**C** and **J**–**L**, respectively. The data in **G** and **P** show two distinct peaks, associated with pMRLC localization at the boundary of the amicrovillar domain in **A** and **J**, respectively. The line scans in **H**, **I**, **Q**, and **R** do not show these distinct peaks. Bar in **L** = 10 μm and is applicable to all images.

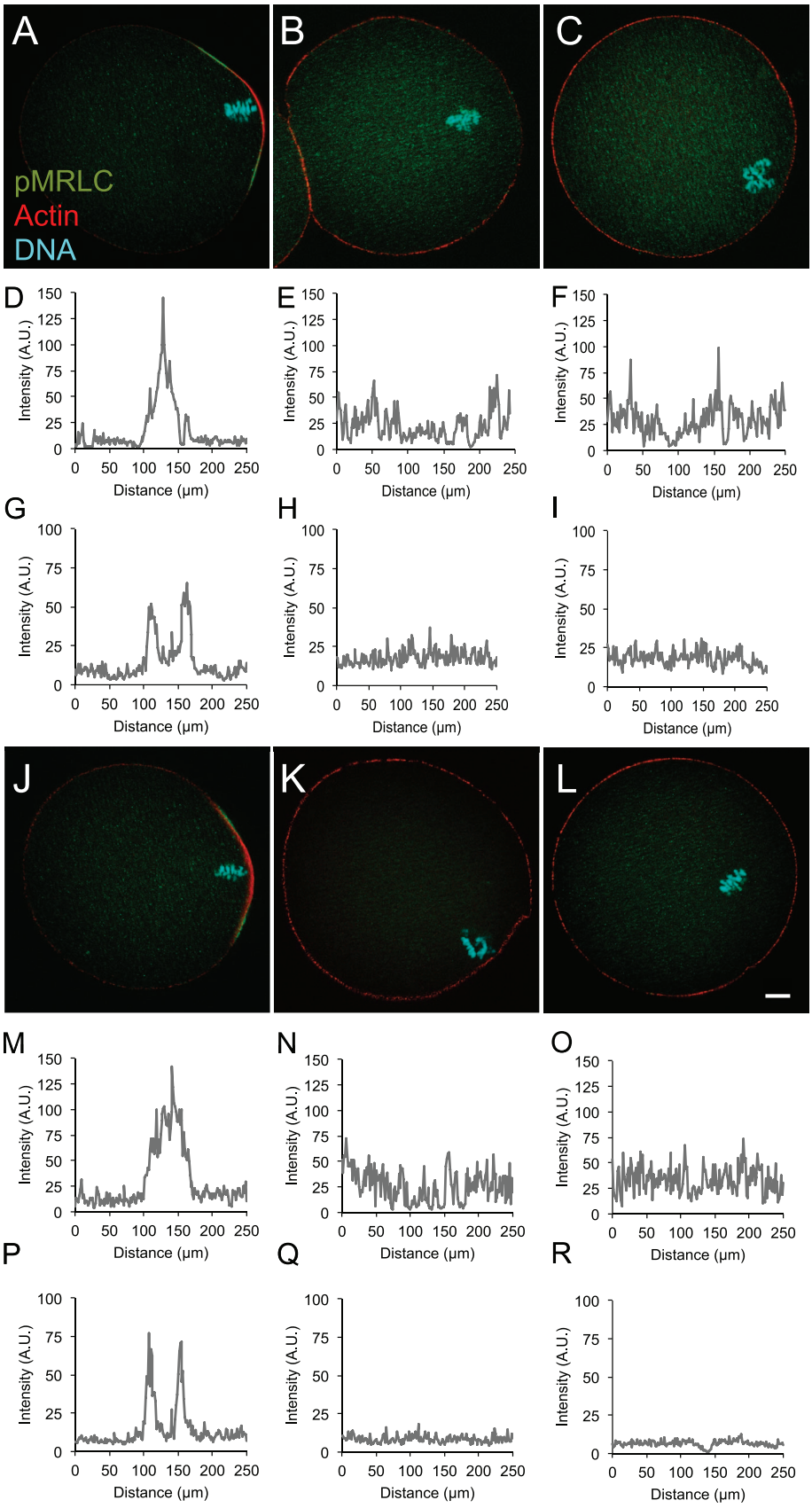

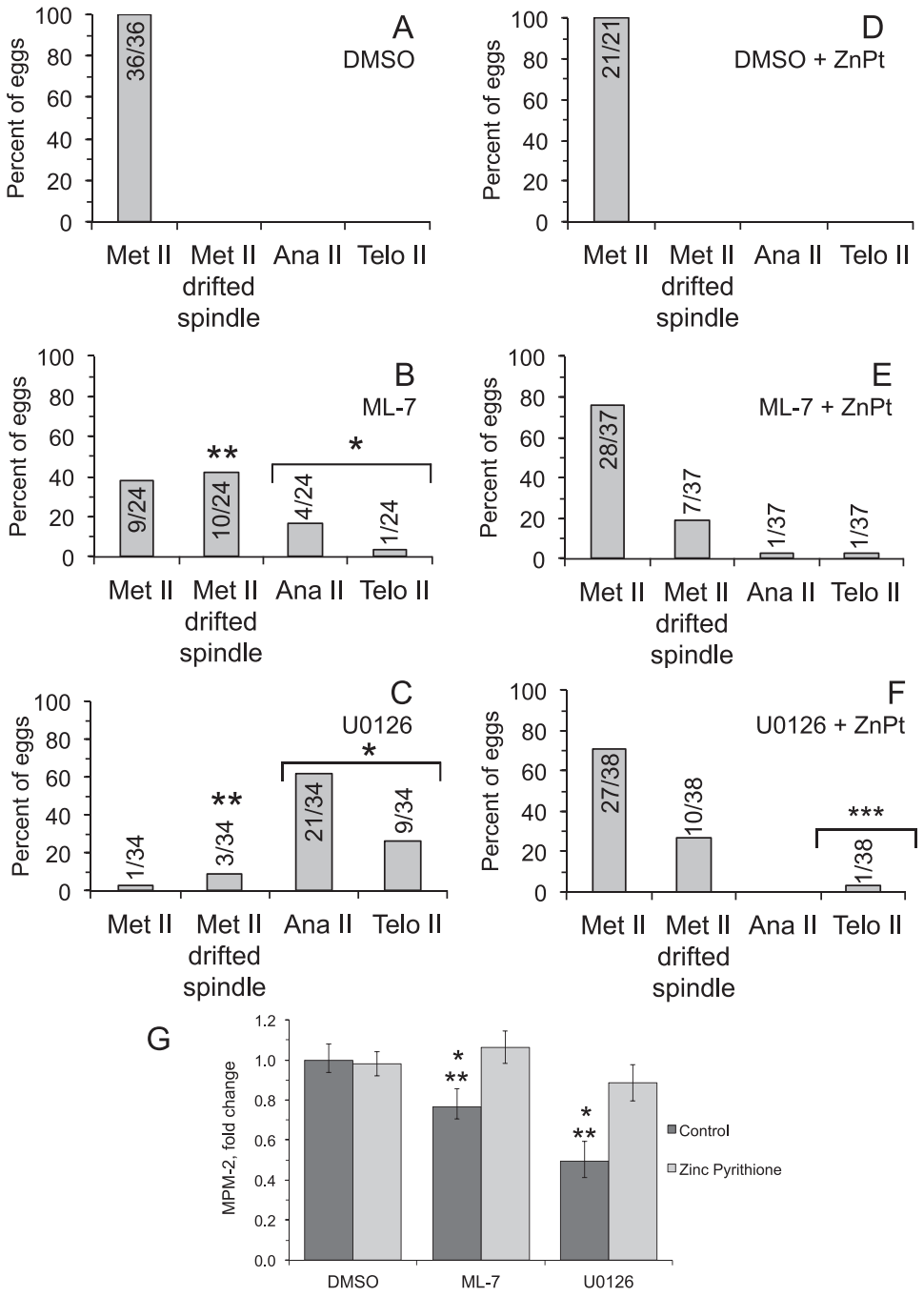

FIG. 7. Effects of zinc ionophore treatment on U0126- and ML-7-induced parthenogenetic exit from metaphase II arrest. For **D**–**F**, metaphase II eggs were hyperloaded with zinc through treatment with 10 μM zinc pyrithione (ZnPT) for 5 min, then treated with 0.5% DMSO, 15 μM ML-7, or 50 μM U0126 for 3 h. In **A**–**C**, control eggs were not treated with ZnPT and simply treated with 0.5% DMSO, 15 μM ML-7, or 50 μM U0126 for 3 h. In **A**–**F**, eggs were analyzed and classified as in Figures 3 and 4: metaphase II, MII drifted spindle (i.e., the DNA was aligned along the metaphase II plate and the spindle was greater than 12 μm from the cortex; shown in Fig. 2), anaphase II, or telophase II (progression out of metaphase II arrest). Numbers in or above the bar indicates numbers of eggs analyzed. The number of eggs that exited from metaphase II arrest following treatment with U0126 is statistically significant compared to U0126-treated eggs that were pretreated with the ZnPT (chi-square analysis, $***P < 0.0001$). Other statistical comparisons: The extent of progression out of metaphase II arrest in U0126- and ML-7-treated eggs is statistically significant as compared to DMSO-treated eggs (chi-square analysis, $*P < 0.0001$). The extent of drifted spindle occurrence in U0126- and ML-7-treated eggs is statistically significant as compared to DMSO-treated eggs (chi-square analysis, $***P < 0.0001$). **G**) Quantification of MPM-2 signals in eggs in the different experimental treatment groups, either not treated with ZnPT (control, dark bars) or treated with ZnPT (light bars). Values were normalized to DMSO-treated control metaphase II eggs. Error bars represent standard error of the mean. Asterisks over the bars indicate distinct statistically significant differences (determined by ANOVA with Fisher's protected least significant different post hoc testing); one asterisk indicates statistically significantly different compared to the group in DMSO and Ca^{2+}-containing medium, and two asterisks indicate statistically significantly different compared to the group in ZnPT-loaded eggs. Number of eggs analyzed, 21–37 per group.

areas should aid understanding of normal egg activation as well as parthenogenesis.

The effects observed with MAPK3/1 pathway inhibition or MLCK inhibition are pertinent to egg health and reproductive success. Loss of maintenance of metaphase II arrest and loss of cortical spindle localization occur with extended time after ovulation as the egg quality deteriorates during a process known as postovulatory aging [14, 15, 90, 91]. Postovulatory aging is associated with unsuccessful fertilization and, in instances when aged eggs are fertilized, with poor reproductive outcomes, including pregnancy loss, smaller litter sizes, or in offspring with abnormalities [14, 15, 90, 91]. Relevant to the data here, postovulatory aged eggs have reduced MAPK3/1 activity associated with a range of membrane and cortical abnormalities and the above-mentioned propensity to undergo parthenogenetic activation [92–100]. Thus, what we observe here with MAPK3/1 pathway inhibition and the associated reduction in myosin-II function is consistent with changes that occur with postovulatory aging, suggestive of a tie between reduced MAPK3/1 activity and several of the changes observed in aged eggs. In conclusion, a functional MAPK3/1 pathway is important for a variety of events in the temporal and spatial regulation of meiosis in mammalian oocytes. The data here provide new insights into the molecular foundations of certain cases of spontaneous egg activation and, more broadly, into the range of functions of MAPK3/1 in mammalian oocytes, consistent with other observations suggestive of coordination of cell cycle progression, cytostatic factor activity, and cytoskeletal regulation [1, 8].

ACKNOWLEDGMENT

We are grateful for expert advice on zinc pyrithione usage from Miranda Bernhardt (NIEHS).

REFERENCES

1. Masui Y, Markert CL. Cytoplasmic control of nuclear behavior during meiotic maturation of frog oocytes. J Exp Zool 1971; 177:129–146.
2. Backs J, Stein P, Backs T, Duncan F, Grueter CE, McAnally J, Qi X, Schultz RM, Olson EN. The gamma isoform of CaM kinase II controls mouse egg activation by regulating cell cycle resumption. Proc Natl Acad Sci U S A 2010; 107:81–86.
3. Oh JS, Susor A, Conti M. Protein tyrosine kinase Wee1B is essential for metaphase II exit in mouse oocytes. Science 2011; 332:462–465.
4. Colledge WH, Carlton MBL, Udy GB, Evans MJ. Disruption of c-mos cause parthenogenetic development of unfertilized mouse eggs. Nature 1994; 370:65–68.
5. Hashimoto N, Watanabe N, Furuta Y, Tamemoto H, Sagata N, Yokoyama M, Okazaki K, Nagayoshi M, Takeda N, Ikawa Y, Aizawa S. Parthenogenetic activation of oocytes in c-mos-deficient mice. Nature 1994; 370:68–71.
6. Verlhac MH, Kubiak JZ, Weber M, Geraud G, Colledge WH, Evans MJ, Maro B. Mos is required for MAP kinase activation and is involved in microtuble organization during meiotic maturation in the mouse. Development 1996; 122:815–822.
7. Yesilaltay A, Dokshin GA, Busso D, Wang L, Galiani D, Chavarria T, Vasile E, Quilaqueo L, Orellana JA, Walzer D, Shalgi R, Dekel N, et al. Excess cholesterol induces mouse egg activation and may cause female infertility. Proc Natl Acad Sci U S A 2014; 111:E4972–E4980.
8. Shoji S, Yoshida N, Amanai M, Ohgishi M, Fukui T, Fujimoto S, Nakano Y, Kajikawa E, Perry AC. Mammalian Emi2 mediates cytostatic arrest and transduces the signal for meiotic exit via Cdc20. EMBO J 2006; 25:834–845.
9. Oh JS, Susor A, Schindler K, Schultz RM, Conti M. Cdc25A activity is required for the metaphase II arrest in mouse oocytes. J Cell Sci 2013; 126:1081–1085.
10. Chung H-Y, Jennings PC, Stewart JL, Verrills NM, Jones KT. Essential role of protein phosphatase 2A in metaphase II arrest and activation of mouse eggs shows by okadaic acid, dominant negative protein phosphatase 2A, and FTY720. J Biol Chem 2011; 286:14705–14712.
11. Suzuki T, Yoshida N, Suzuki E, Okuda E, Perry ACF. Full-term mouse development by abolishing Zn^{2+}-dependent metaphase II arrest without Ca^{2+} release. Development 2010; 137:2659–2669.
12. Kim AM, Bernhardt ML, Kong BY, Ahn RW, Vogt S, Woodruff TK, O'Halloran TV. Zinc sparks are triggered by fertilization and facilitate cell cycle resumption in mammalian eggs. ACS Chem Biol 2011; 6: 716–723.
13. Bernhardt ML, Kong BY, Kim AM, O'Halloran TV, Woodruff TK. A zinc-dependent mechanism regulates meiotic progression in mammalian oocytes. Biol Reprod 2012; 86:114.
14. Marston JH, Chang MC. The fertilizable life of ova and their morphology following delayed insemination in mature and immature mice. J Exp Zool 1964; 155:237–252.
15. Lord T, Aitken RJ. Oxidative stress and ageing of the post-ovulatory oocyte. Reproduction 2013; 146:R217–R227.
16. Ubaldi FM, Rienzi L. Morphological selection of gametes. Placenta 2008; 29(Suppl B):115–120.
17. De Santis L, Cino I, Rabellotti E, Calzi F, Persico P, Boroni A, Coticchio G. Polar body morphology and spindle imaging as predictors of oocyte quality. Reprod Biomed Online 2005; 11:36–42.
18. Sharan SK, Pyle A, Coppola V, Babus J, Swaminathan S, Benedict J, Swing D, Martin BK, Tessarollo L, Evans JP, Flaws JA, Handel MA. BRCA2 deficiency in mice leads to meiotic impairment and infertility. Development 2004; 131:131–142.
19. Levi M, Maro B, Shalgi R. The involvement of Fyn kinase in resumption of the first meiotic division in mouse oocytes. Cell Cycle 2010; 9: 1577–1589.
20. Luo J, McGinnis LK, Kinsey WH. Role of Fyn kinase in oocyte developmental potential. Reprod Fertil Dev 2010; 22:966–976.
21. Jones KT. Anaphase-promoting complex control in female mouse meiosis. Results Probl Cell Differ 2011; 53:343–363.
22. Homer H. The APC/C in female mammalian meiosis I. Reproduction 2013; 146:R61–R71.
23. Pines J. Mitosis: a matter of getting rid of the right protein at the right time. Trends Cell Biol 2006; 16:55–63.
24. Tung JJ, Hansen DV, Ban KH, Loktev AV, Summers MK, Adler JR III, Jackson PK. A role for the anaphase-promoting complex inhibitor Emi2/XErp1, a homolog of early mitotic inhibitor 1, in cytostatic factor arrest of Xenopus eggs. Proc Natl Acad Sci U S A 2005; 102:4318–4323.
25. Hirao Y, Eppig JJ. Parthenogenetic development of Mos-deficient mouse oocytes. Mol Reprod Dev 1997; 48:391–396.
26. Phillips KP, Petrunewich MA, Collins JL, Booth RA, Liu XJ, Baltz JM. Inhibition of MEK or cdc2 kinase parthenogenetically activates mouse eggs and yields the same phenotypes as Mos(-/-) parthenogenotes. Dev Biol 2002; 247:210–223.
27. Tong C, Fan HY, Chen DY, Song XF, Schatten H, Sun QY. Effects of MEK inhibitor U0126 on meiotic progression in mouse oocytes: microtuble organization, asymmetric division and metaphase II arrest. Cell Res 2003; 13:375.
28. Miyagaki Y, Kanemori Y, Tanaka F, Baba T. Possible role of p38 MAPK-MNK1-EMI2 cascade in metaphase-II arrest of mouse oocytes. Biol Reprod 2014; 91:45.
29. Suzuki T, Suzuki E, Yoshida N, Kubo A, Li H, Okuda E, Amanai M, Perry ACF. Mouse Emi2 as a distinctive regulatory hub in second meiotic metaphase. Development 2010; 137:3281–3291.
30. Ducibella T, Fissore R. The roles of Ca^{2+}, downstream protein kinases, and oscillatory signaling in regulating fertilization and the activation of development. Dev Biol 2008; 315:257–279.
31. Miao Y-L, Williams CJ. Calcium signaling in mammalian egg activation and embryo development: the influence of subcellular localization. Mol Reprod Dev 2012; 79:742–756.
32. Chang H-Y, Minahan K, Merriman JA, Jones KT. Calmodulin-dependent protein kinase gamma3 (CamKIIg3) mediates the cell cycle resumption of metaphase II eggs in mouse. Development 2009; 136: 4077–4081.
33. Medvedev S, Stein P, Schultz RM. Specificity of calcium/calmodulin-dependent protein kinases in mouse egg activation. Cell Cycle 2014; 13: 1482–1488.
34. Rauh NR, Schmidt A, Bormann J, Nigg EA, Mayer TU. Calcium triggers exit from meiosis II by targeting the APC/C inhibitor XErp1 for degradation. Nature 2005; 437:1048–1052.
35. Verlhac MH, Kubiak JZ, Clarke HJ, Maro B. Microtubule and chromatin behavior follow MAP kinase activity but not MPF activity during meiosis in mouse oocytes. Development 1994; 120:1017–1025.
36. Moos J, Visconti PE, Moore GD, Schultz RM, Kopf GS. Potential role of mitogen-activated protein kinase in pronuclear envelope assembly and disassembly following fertilization of mouse eggs. Biol Reprod 1995; 53: 692–699.

37. Petrunewich MA, Trimarchi JR, Hanlan AK, Hammer MA, Baltz JM. Second meiotic spindle integrity requires MEK/MAP kinase activity in mouse eggs. J Reprod Dev 2009; 55:30–38.
38. Gonzalez-Garcia JR, Bradley J, Nomikos M, Paul L, Machaty Z, Lai FA, Swann K. The dynamics of MAPK inactivation at fertilization in mouse eggs. J Cell Sci 2014; 127:2749–2760.
39. Choi TS, Fukasawa K, Zhou RP, Tessarollo L, Borror K, Resau J, Vande Woude GF. The Mos/mitogen-activated protein kinase (MAPK) pathway regulates the size and degradation of the first polar body in maturing mouse oocytes. Proc Natl Acad Sci U S A 1996; 93:7032–7035.
40. Chaigne A, Campillo C, Gov NS, Voituriez R, Azoury J, Umaña-Diaz C, Almonacid M, Queguiner I, Nassoy P, Sykes C, Verlhac M-H, Terret M-E. A soft cortex is essential for asymmetric spindle positioning in mouse oocytes. Nat Cell Biol 2013; 15:958–966.
41. Klemke RL, Cai S, Giannini AL, Gallagher PJ, de Lanerolle P, Cheresh DA. Regulation of cell motility by mitogen-activated protein kinase. J Cell Biol 1997; 137:481–492.
42. Nguyen DH, Catling AD, Webb DJ, Sankovic M, Walker LA, Somlyo AV, Weber MJ, Gonias SL. Myosin light chain kinase functions downstream of Ras/ERK to promote migration of urokinase-type plasminogen activator-stimulated cells in an integrin-selective manner. J Cell Biol 1999; 146:149–164.
43. Vicente-Manzanares M, Ma X, Adelstein RS, Horwitz AF. Non-muscle myosin II take centre stage in cell adhesion and migration. Nat Rev Mol Cell Biol 2009; 10:778–790.
44. Larson SM, Lee HJ, Hung PH, Matthews LM, Robinson DN, Evans JP. Cortical mechanics and meiosis II completion in mammalian oocytes are mediated by myosin-II and Ezrin-Radixin-Moesin (ERM) proteins. Mol Biol Cell 2010; 21:3182–3192.
45. Azoury J, Lee KW, Georget V, Hikal P, Verlhac MH. Symmetry breaking in mouse oocytes requires transient F-actin meshwork destabilization. Development 2011; 138:2903–2908.
46. Simerly C, Nowak G, de Lanerolle P, Schatten G. Differential expression and functions of cortical myosin IIA and IIB isotypes during meiotic maturation, fertilization, and mitosis in mouse oocytes and embryos. Mol Biol Cell 1998; 9:2509–2525.
47. Schuh M, Ellenberg J. A new model for asymmetric spindle positioning in mouse oocytes. Curr Biol 2008; 18:1986–1992.
48. Deng M, Williams CJ, Schultz RM. Role of MAP kinase and myosin light chain kinase in chromosome-induced development of mouse egg polarity. Dev Biol 2005; 278:358–366.
49. Matson S, Markoulaki S, Ducibella T. Antagonists of myosin light chain kinase and of myosin II inhibit specific events of egg activation in fertilized mouse eggs. Biol Reprod 2006; 74:169–176.
50. Deng M, Suraneni P, Schultz RM, Li R. The Ran GTPase mediates chromatin signaling to control cortical polarity during polar body extrusion in mouse oocytes. Dev Cell 2007; 12:301–308.
51. Ajduk A, Ilozue T, Windsor S, Yu Y, Seres KB, Bomphrey RJ, Tom BD, Swann K, Thomas A, Graham CF, Zernicka-Goetz M. Rhythmic actomyosin-driven contractions induced by sperm entry predict mammalian embryo viability Nat Commun 2011; 2:417.
52. Whitten WK. Nutrient requirements for the culture of preimplantation embryos in vitro. Adv Biosci 1971; 6:129–141.
53. Favata MF, Horiuchi KY, Manos EJ, Daulerio AJ, Stradley DA, Feeser WS, Van Dyk DE, Pitts WJ, Earl RA, Hobbs F, Copeland RA, Magolda RL, et al. Identification of a novel inhibitor of mitogen-activated protein kinase kinase. J Biol Chem 1998; 273:18623–18632.
54. Yu LZ, Xiong B, Gao WX, Wang CM, Zhong ZS, Huo LJ, Wang Q, Hou Y, Liu K, Liu XJ, Schatten H, Chen DY, et al. MEK1/2 regulates microtubule organization, spindle pole tethering and asymmetric division during mouse oocyte meiotic maturation. Cell Cycle 2007; 6:330–338.
55. Nabti I, Marangos P, Bormann J, Kudo NR, Carroll J. Dual-mode regulation of the APC/C by CDK1 and MAPK controls meiosis I progression and fidelity. J Cell Biol 2014; 204:891–900.
56. Markoulaki S, Matson S, Ducibella T. Fertilization stimulates long-lasting oscillations of CaMKII activity in mouse eggs. Dev Biol 2004; 272:15–25.
57. Kolega J. Phototoxicity and photoinactivation of blebbistatin in UV and visible light. Biochem Biophys Res Commun 2004; 320:1020–1025.
58. Gardner AJ, Williams CJ, Evans JP. Establishment of the mammalian membrane block to polyspermy: evidence for calcium-dependent and -independent regulation. Reproduction 2007; 133:383–393.
59. Kryzak CA, Moraine MM, Kyle DD, Lee HJ, Cubeñas-Potts C, Robinson DN, Evans JP. Prophase I mouse oocytes are deficient in the ability to respond to fertilization by decreasing membrane receptivity to sperm and establishing a membrane block to polyspermy. Biol Reprod 2013; 89:44.
60. Evans JP, Schultz RM, Kopf GS. Mouse sperm-egg membrane interactions: analysis of roles of egg integrins and the mouse sperm homologue of PH-30 (fertilin). J Cell Sci 1995; 108:3267–3278.
61. Taki M, Wolford JL, O'Halloran TV. Emission ratiometric imaging of intracellular zinc: design of a benzoxazole fluorescent sensor and its application in two-photon microscopy. J Am Chem Soc 2004; 126: 712–713.
62. Davis FM, Tsao TY, Fowler SK, Rao PN. Monoclonal antibodies to mitotic cells. Proc Natl Acad Sci U S A 1983; 80:2926–2930.
63. McGinnis LK, Albertini DF. Dynamics of protein phosphorylation during meiotic maturation. J Assist Reprod Genet 2010; 27:169–182.
64. Li H, Guo F, Rubinstein B, Li R. Actin-driven chromosomal motility leads to symmetry breaking in mammalian meiotic oocytes. Nat Cell Biol 2008; 10:1301–1308.
65. Derganc J, Božic B, Sventina S, Žekš B. Stability analysis of micropipette aspiration of neutrophils. Biophys J 2000; 79:153–162.
66. Reichl EM, Ren Y, Morphew MK, Delannoy M, Effler JC, Girard KD, Divi S, Iglesias PA, Kuo SC, Robinson DN. Interactions between myosin and actin crosslinkers control cytokinesis contractility dynamics and mechanics. Curr Biol 2008; 18:471–480.
67. Miao Y-L, Stein P, Jefferson WN, Padilla-Banks E, Williams CJ. Calcium influx-mediated signaling is required for complete mouse egg activation. Proc Natl Acad Sci U S A 2012; 109:4169–4174.
68. Horner VL, Wolfner MF. Mechanical stimulation by osmotic and hydrostatic pressure activates *Drosophila* oocytes in vitro in a calcium-dependent manner. Dev Biol 2008; 316:100–109.
69. Kaneuchi T, Sartain CV, Takeo S, Horner VL, Buehner NA, Aigaki T, Wolfner MF. Calcium waves occur as *Drosophila* oocytes activate. Proc Natl Acad Sci U S A 2015; 112:791–796.
70. Kline D, Kline JT. Repetitive calcium transients and the role of calcium in exocytosis and cell cycle activation in the mouse egg. Dev Biol 1992; 149:80–89.
71. Verlhac M-H, De Pennett H, Maro B, Cobb M, Clarke HJ. MAP kinase becomes stably activated at metaphase and is associated with microtubule-organizing centers during meiotic maturation of mouse oocytes. Dev Biol 1993; 158:330–340.
72. Verlhac MH, Lefebvre C, Kubiak JZ, Umbhauer M, Rassinier P, Colledge W, Maro B. Mos activates MAP kinase in mouse oocytes through two opposite pathways. EMBO J 2000; 19:6065–6074.
73. Halet G, Carroll J. Rac activity is polarized and regulates meiotic spindle stability and anchoring in mammalian oocytes. Dev Cell 2007; 12: 309–317.
74. Yi K, Unruh JR, Deng M, Slaughter BD, Rubinstein B, Li R. Dynamic maintenance of asymmetric meiotic spindle position through ARP2/3-complex-driven cytoplasmic streaming in mouse oocytes. Nat Cell Biol 2011; 13:1252–1258.
75. Que EL, Bleher R, Duncan FE, Kong BY, Gleber SC, Vogt S, Chen S, Garwin SA, Bayer AR, Dravid VP, Woodruff TK, O'Halloran TV. Quantitative mapping of zinc fluxes in the mammalian egg reveals the origin of fertilization-induced zinc sparks. Nat Chem 2015; 7:130–139.
76. Tahara M, Tasaka K, Masumoto N, Mammoto A, Ikebuchi Y, Miyake A. Dynamics of cortical granule exocytosis at fertilization in living mouse eggs. Am J Physiol 1996; 270:C1354–C1361.
77. DiMaggio AJ Jr, Lonergan TA, Stewart-Savage J. Cortical granule exocytosis in hamster eggs requires microfilaments. Mol Reprod Dev 1997; 47:334–340.
78. Terada Y, Simerly C, Schatten G. Microfilament stabilization by jasplakinolide arrests oocyte maturation, cortical granule exocytosis, sperm incorporation cone resorption, and cell-cycle progression, but not DNA replication, during fertilization in mice. Mol Reprod Dev 2000; 56: 89–98.
79. Lichten LA, Cousins RJ. Mammalian zinc transporters: nutritional and physiologic regulation. Annu Rev Nutr 2009; 29:153–176.
80. Kambe T. Molecular architecture and function of ZnT transporters. Curr Top Membr 2012; 69:199–220.
81. Dempski RE. The cation selectivity of the ZIP transporters. Curr Top Membr 2012; 69:221–245.
82. Yao Y, Ferrer-Montiel AV, Montal M, Tsien RY. Activation of store-operated Ca2+ current in Xenopus oocytes requires SNAP-25 but not a diffusible messenger. Cell 1999; 98:475–485.
83. Bezzerides VJ, Ramsey IS, Kotecha S, Greka A, Clapham DE. Rapid vesicular translocation and insertion of TRP channels. Nat Cell Biol 2004; 6:709–720.
84. Meyer NE, Joel-Almagor T, Frechter S, Minke B, Huber A. Subcellular translocation of the eGFP-tagged TRPL channel in Drosophila photoreceptors requires activation of the phototransduction cascade. J Cell Sci 2006; 119:2592–2603.

85. Monet M, Francoeur N, Boulay G. Involvement of phosphoinositide 3-kinase and PTEN protein in mechanism of activation of TRPC6 protein in vascular smooth muscle cells. J Biol Chem 2012; 287:17672–17681.
86. Gu Y, Gu C. Physiological and pathological functions of mechanosensitive ion channels. Mol Neurobiol 2014; 50:339–347.
87. Martinac B. The ion channels to cytoskeleton connection as potential mechanism of mechanosensitivity. Biochim Biophys Acta 2014; 1838: 682–691.
88. Plant TD. TRPs in mechanosensing and volume regulation. Handb Exp Pharmacol 2014; 223:743–766.
89. Carvacho I, Lee HC, Fissore RA, Clapham DE. TRPV3 channels mediate strontium-induced mouse-egg activation. Cell Rep 2013; 5:1375–1386.
90. Tarin JJ, Perez-Albala S, Cano A. Consequences on offspring of abnormal function in ageing gametes. Hum Reprod Update 2000; 6: 532–549.
91. Fissore RA, Kurokawa M, Knott J, Zhang M, Smyth J. Mechanisms underlying oocyte activation and postovulatory aging. Reproduction 2002; 124:745–754.
92. Szollosi D. Morphological changes in mouse eggs due to aging in the fallopian tube. Am J Anat 1971; 130:209–225.
93. Longo FJ. Ultrastructural changes in rabbit eggs aged in vivo. Biol Reprod 1974; 11:22–39.
94. Webb M, Howlett SK, Maro B. Parthenogenesis and cytoskeletal organization in ageing mouse eggs. J Embryol Exp Morphol 1986; 95: 131–145.
95. Eichenlaub-Ritter U, Chandley AC, Gosden RG. Alterations to the microtubular cytoskeleton and increased disorder of chromosome alignment in spontaneously ovulated mouse oocytes aged in vivo: an immunofluorescence study. Chromosoma 1986; 94:337–345.
96. Goud AP, Goud PT, Diamond MP, Van Oostveldt P, Hughes MR. Microtubule turnover in ooplasm biopsy reflects ageing phenomena in the parent oocyte. Reprod Biomed Online 2005; 11:43–52.
97. Xu Z, Abbott A, Kopf GS, Schultz RM, Ducibella T. Spontaneous activation of ovulated mouse eggs: time-dependent effects on M-phase exit, cortical granule exocytosis, maternal messenger ribonucleic acid recruitment, and inositol 1,4,5-trisphosphate sensitivity. Biol Reprod 1997; 57:743–750.
98. Mailhes JB, Young D, London SN. Postovulatory aging of mouse oocytes in vivo and premature centromere separation and aneuploidy. Biol Reprod 1998; 58:1206–1210.
99. Dalo DT, McCaffery JM, Evans JP. Ultrastructural analysis of egg membrane abnormalities in post-ovulatory aged eggs. Int J Dev Biol 2008; 52:535–544.
100. Wortzman GB, Evans JP. Membrane and cortical abnormalities in post-ovulatory aged eggs: analysis of fertilizability and establishment of the membrane block to polyspermy. Mol Hum Reprod 2005; 11:1–9.